Acoustic Assessment of Lithium-Ion Batteries: Unravelling Temperature and Charge Contributions

Daniel Williams[a], Robert Milton[b], Joshua Taylor[b], Robert Dwyer-Joyce[a], Solomon Brown[b,*]

[a]*School of Mechanical, Aerospace and Civil Engineering, The University of Sheffield, Mappin Street, S1 3JD, UK*
[b]*School of Chemical Material and Biological Engineering, The University of Sheffield, Mappin Street, Sheffield, S1 3JD, UK*

Abstract

Lithium-ion batteries (LIBs) are critical for renewable energy storage, and accurate charge and health estimation remains a significant challenge. Acoustic sensing offers a unique method to observe lithium-ion movement between electrodes during battery operation. However, both the charge state and the internal temperature of the battery affect the acoustic response.

This study systematically investigates the interactions between temperature and charge state on acoustic signals through a novel thermal cycle methodology. Using a global sensitivity analysis, we demonstrate that temperature has a non-negligible and dominant effect on the acoustic signal, with a largely insignificant cooperative interaction with charge state. The results reveal temperature-induced variations in the acoustic signal that increase with charge level, though not uniformly.

Our findings underscore the critical importance of temperature compensation in acoustic-based LIB estimation techniques. By quantifying the independent and cooperative effects of temperature and charge, this research provides the possibility of independently measuring thermal and SOC effects on the acoustic signal without the need for additional thermal sensing equipment.

Keywords: Lithium-ion battery; Ultrasonic acoustics; Global sensitivity analysis; Gaussian processing

1. Introduction

Lithium-ion batteries (LIBs) have emerged as a transformative energy storage technology since their commercial introduction by Sony in 1991. Characterized by high energy and power densities, extended cycle life, and minimal self-discharge [1–3], LIBs have become the dominant battery chemistry across portable electronics and the rapidly expanding electric vehicle (EV) market [4, 5]. This technological advancement presents a critical pathway to decar-

*Corresponding author
Email address: s.f.brown@sheffield.ac.uk, +44 114 222 7597, Professor Solomon Brown, School of Chemical, Material and Biological Engineering, Sir Robert Hadfield Building Mappin Street Sheffield S1 3JD (Solomon Brown)

bonizing transportation, which currently accounts for 12% of global greenhouse gas emissions[6].

Despite widespread adoption, LIBs face significant challenges in real-time monitoring and safety. This is despite a low failure margin of 1 in 10-40 million batteries [7, 8]. Battery Management Systems (BMSs) have been developed to address these concerns, employing various sophisticated techniques such as neural networks and support vector machines working from a large real dataset [9], models such as the Thevenin model using open-circuit voltage measurements [10], and Coulomb counting [11].

These methods have been successfully implemented in real-world situations, but all of them are monitoring variables, such as cell voltage, current, and surface temperature [12], that are externally monitored from the cell; they are unable to monitor the movement of Li^+ which is the driving mechanism for LIB operation. The movement of Li^+ between the electrodes is assumed from electrical and electrochemical models [13]. These electrochemical systems use physics-based methods to provide information on the internal electrochemical dynamics of a LIB [14]. These models have been used to monitor changes in the electrochemical parameters such as terminal voltage [15, 16], detecting abusive operating conditions [17] and cell ageing [18]. However, these methods model the internal changes, albeit with high accuracy. Direct monitoring of the internal changes are not implemented with these models, as the external electrochemical variables such as the cell voltage or current and estimate them through the use of physics [14].

To address this gap, acoustic monitoring has emerged as a promising answer to direct monitoring of the internal dynamics. First introduced by Sood in 2014 [19], ultrasonic monitoring offers a unique approach to battery estimation by monitoring Li^+ movement between the electrodes causing material property changes during battery operation. These changes, primarily in bulk and shear moduli and density, directly influence acoustic wave propagation speed through a medium, allowing for indirect yet precise observation of electrochemical processes. The sound propagation speed is defined as:

$$c = \sqrt{\frac{K + \frac{4}{3}G}{\rho}} \tag{1}$$

Where: c = Speed of sound (m s^{-1}) - K = Bulk modulus (GPa) - G = Shear modulus (GPa) - ρ = Density of the material (kg m^{-3})

At each interface between two media, part of the acoustic wave will transmit into the new medium and part will be reflected. The ratio of the transmitted signal to reflected signal is dependant on the difference in acoustic impedances (Z) of the two media. This is called the reflection coefficient (R), and is defined as:

$$R = \frac{Z_2 - Z_1}{Z_2 + Z_1} \tag{2}$$

where Z is defined as:

$$Z = \rho \times c \tag{3}$$

As the signal splits when interacting with an interface, the signal amplitude decreases with respect to the ratio of transmission to reflection. The signal also sees attenuation as it travels through a medium [20], and this can be defined as:

$$A = A_0 e^{-\alpha d} \tag{4}$$

Where: A = Final acoustic amplitude - A_0 = Initial acoustic amplitude - α= Attenuation coefficient - d = Distance travelled by the wave (m)

This can be observed as absorption, which is the conversion of acoustic energy into heat in the host medium.

As the speed of sound is affected by the changes in material properties, the time-of-flight (TOF) of the battery is also affected. This makes it a useful ultrasonic property for monitoring SOC, and will be explored within this work.

The relationship between TOF and SOC is known in the literature to be linear [21, 22], as a result of the linear changes to the elastic moduli [23, 24] and volumetric expansion [25–27] of the electrodes with respect to Li concentration. Equation 1 illustrates that the elastic moduli and density that are proportional to the speed of sound, and therefore the TOF. There are other variables that can affect the TOF in LIBs. The state-of-health (SOH) can permanently shift the base TOF as the cell degrades [28], which can differ between cathode chemistries [29, 30]; defects within the cell can notably alter the response [31]; and the internal structures of the cells can affect the signal, such as the number of layers [32].

Temperature, in comparison, has received less interest with regard to acoustic LIB monitoring, except for a few articles [33–35] developing methods to decouple and monitor temperature and charge during operation for thermal runaway detection. These have been summarised in Table 1. Temperature is known to cause thermal expansion and affect the way acoustic waves travel through different media, with an increase in temperature decreasing the speed of sound through a medium [36].

$$dL = L_0 \alpha (T_1 - T_0) \tag{5}$$

Where: dL = Change in Length (m) - L_0 = Initial Length (m) - α = Thermal expansion coefficient (K^{-1}) - T_1 = Final temperature (K) - T_0 = Initial temperature (K)

The electrodes have been found to expand mostly linearly with temperature [37, 38], which increases the travel path for the ultrasonic waves resulting in a longer TOF if all other variables are constant. However, research is not in total agreement over the effects of temperature on TOF measurements. Some reports state temperature is not a significant variable to consider [39] whilst others state ultrasonic waves can be more sensitive to temperature than charge [40, 41].

In this study, we investigated the effects of temperature and charge on the acoustic signal when monitoring LIBs, both independently and combined. This was to determine the dependence or independence of the two variables upon the acoustic signal. In order to carry this out, a method of thermally cycling cells at different states-of-charge (SOCs) while recording the acoustic signal was used to create a matrix of data points of temperature, battery charge, and acoustics. Multiple cells were used in this study. We found that temperature and the TOF have a linear correlation - as temperature increases, the TOF increases. Charge has an inverse relationship with the TOF, as an increase in SOC results in a decrease in TOF. The two variables are mostly independent from one another when looking at the change in TOF, meaning that a change in temperature would cause a similar change in the TOF when performed at different SOCs. Our research not only addresses the current knowledge gap regarding temperature effects but also provides a foundational framework for improving the accuracy and reliability of acoustic monitoring techniques across different lithium-ion battery chemistries.

Table 1: Papers Addressing Temperature and TOF in LIBs.

Findings	Reference
Ultrasonic TOF was corrected for temperature effects using -10, 25 and 60 °C	[33]
Ultrasonic TOF can be used to detect temperature fluctuations	[34]
Corrected temperature effects on TOF for the use of detecting thermal runaway based on overcharging cells	[35]

2. Methodology

2.1. Materials and equipment

All pouch cells (NMC811/graphite) were purchased from RS Pro with stock number 125-1266, and were tested without further modifications. The cells were commercial lithium-ion pouch batteries with a capacity of 2000 mA h and a voltage range of 3.0 - 4.2 V. The cells had an NMC cathode and a graphite anode. The cells had dimensions of 63 x 43.5 x 7 mm and a weight of 40 g. The cells were from the same manufacturing batch and nominally are identical. The piezoelectric transducers were purchased from Del Piezo Specialties, and had a central frequency of

2 MHz. This frequency was determined based on previous work, outlined in [42], where 2 - 2.5 MHz was found to provide an acceptable balance between the sensitivity of the signal to internal changes, and the resistance of the signal to attenuation. These values, along with the experimental parameters are shown in Table 2. The M-Bond 200 adhesive was purchased from Micro Measurements. The K-type thermocouples were purchased from RS Pro with stock number 621-2170. The Picoscope 5444D oscilloscope was purchased from Pico Technology.

2.2. Instrumentation

Piezoelectric transducers were bonded to the centre of a cell's surface using the M-Bond 200 adhesive at room temperature. The transducers were wrap-around as the cells were housed in plastic cases. The positive and negative electrode were both accessible from the top of the transducer, making the soldering of co-axial wires possible. The co-axial wires were stripped and the positive and negative cables were separated to be soldered onto the transducer electrodes. The thermocouples were attached to the surface of the cells using electrical tape. The transducer acted as a transmitter and receiver of the acoustic signal and was controlled by the Picoscope. The acquisition time was once a minute for all data types. The acoustic data was recorded for one second every minute and each capture recorded 50 pulses.

2.3. Thermal and charge cycling

The cells were thermally cycled in a MACCOR MTC-020 temperature chamber. The temperature was cycled in 5 °C steps, starting at 20 °C. The temperature was dropped to 10 °C, increased to 50 °C and returned to 20 °C, see Figure 1. The target temperatures were held for one hour. This provided a rest time for the cells to reach the target temperature and data collection. In order to negate the resting period for data analysis, a range of ±0.3 °C for the cell surface temperature was used to discriminate between resting data and thermally stable. The target temperature range was selected to test the effects of temperature on the acoustic signal within the normal battery operating temperatures. Temperature based degradation, such as SEI decomposition at ~80 °C and lithium plating at ~−20 °C were avoided to reduce additional influences on the acoustic signal. This thermal cycle was performed at various cell SOCs, increasing from 0% to 100% in 20% steps. The cells were charged in this manner using a MACCOR Model 3650 battery cycler. The cells were charged with a current of 0.3 C between 3 and 4.2 V.

2.4. Data analysis

Acoustic and temperature data were recorded using a bespoke LabVIEW VI, and the battery data was recorded using the MACCOR software. The acoustic data was averaged across the 50 pulses and filtered using MATLAB's *wdenoise* denoising function, applying a high-pass filter. A peak tracking method was used to identify each peak in the acoustic response and track their movement, both the amplitude and TOF, throughout the experiment [43]. Tracking

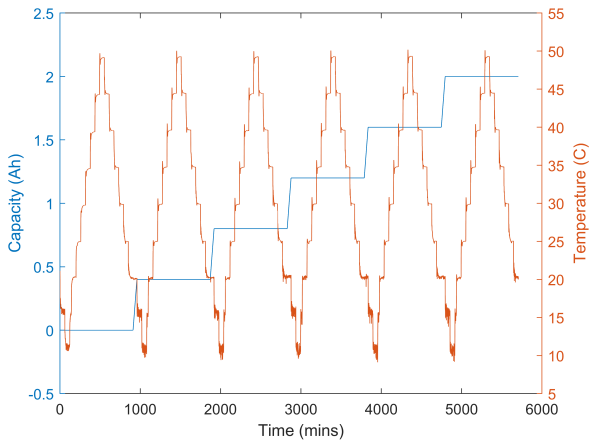

Figure 1: Visualisation of the charge and thermal cycling scheme.

the individual peaks provides the ability to determine if and how the amount of cell exposure affects the signal.

Sensitivity analysis was performed in Python using the *romcomma* package. This package utilises global sensitivity analysis and Gaussian process regression to create a reduced order model [44]. Here, we employed the Sobol' index, a variance-based method that quantifies the individual and codependent contributions of the charge and temperature on the TOF. The Sobol' indices are computed by partitioning the total variance of the model output into components corresponding to each input parameter, as well as their interactions. For an input variable, the first-order Sobol' index represents the fraction of the output variance attributable solely to the variation in while higher-order, in this case total-order indices, capture the influence of interactions between multiple input factors. These indices are calculated through Monte Carlo sampling, where a large number of input-output pairs are generated to estimate the contribution of each input factor. The data underwent 27 k-folds, 26 of which were training datasets and the 27th was the final fold.

In this work, the GSA was used to detect the influence of the temperature and the SOC - based on the spread of the Li-ions between electrodes - on the acoustic signal. The input variables were the SOC and the surface temperature of the cells, and the output variable was the TOF measurements. The first order Sobol' indices contained the effect that the SOC and temperature had independently on the TOF. The second order Sobol' indices contained the co-dependent effects of both SOC and temperature on the TOF.

Table 2: Cell and Test Design Parameters.

Parameter	Value
Cell Capacity	2000 mAh
Cell Chemistry	NMC
SOC Step Increment	Increase of 20%
Charge Rate	0.3C
Voltage Range	3.0-4.2 V
Temperature Range	10 - 50 °C
Temperature Step Increments	Change of ±5 °C
Number of Discrete Points	54 - Nine Temperature at Six SOC
Time Held at Each Discrete Point	One Hour
Age of Cells	Fresh
Number of Full Charge Cycles	Zero - cells were only charged
Form Factor	Jelly Roll
Sensor Central Frequency	2 MHz

3. Results

3.1. Finding the acoustic influences

By thermally and electrochemically cycling the cells, the influence of each on the acoustic response could be determined. We propose that controlling these two parameters (temperature and charge) at stable points creates a discrete matrix to isolate their influences, with the acoustic signal captured via piezoelectric crystal in pulse-echo mode to characterise the internal active layers (Figure 2a). The temperature and charge of the cells were adjusted over a long time-frame to ensure uniformity of internal temperature and lithium-ion movement, respectively.

The resultant acoustic signal (A-Scan) from one of the cells (Figure 2b) shows multiple clear echoes where the initial pulse has travelled through the cell and reflected from individual active layers, such the separators and electrodes, and the back wall. The increase in amplitude at ca. 13 µs signifies the first echo (with preceding peaks resulting from transducer damping), whilst the amplitudes and TOFs of the first and second identified echo groups suggest an acoustic barrier within the cell. This is to be expected, as the cells were prismatically wound, creating a pool of electrolyte in the centre of the cell. Given the prismatic winding design of the cells, it can be assumed that every 2 n - 1 echoes are half echoes, as the signal would split at the pool due to greater differences in acoustic impedances between the electrolyte and the active materials. As these echoes contain information for at least half of the cell, they can still be used for analysis. This also implies that the resultant acoustic echoes are a superposition of multiple reflections from individual layers within the cell, rather than each echo correlating to a specific layer or active component [43].

The surface plot of the signal for one thermal cycle demonstrates the significant effect temperature has on the acoustic signal (Figure 2c). The transitions between stable temperature points are clearly visible within the plot, with TOF increasing and decreasing in distinct increments alongside temperature changes; each step was maintained for

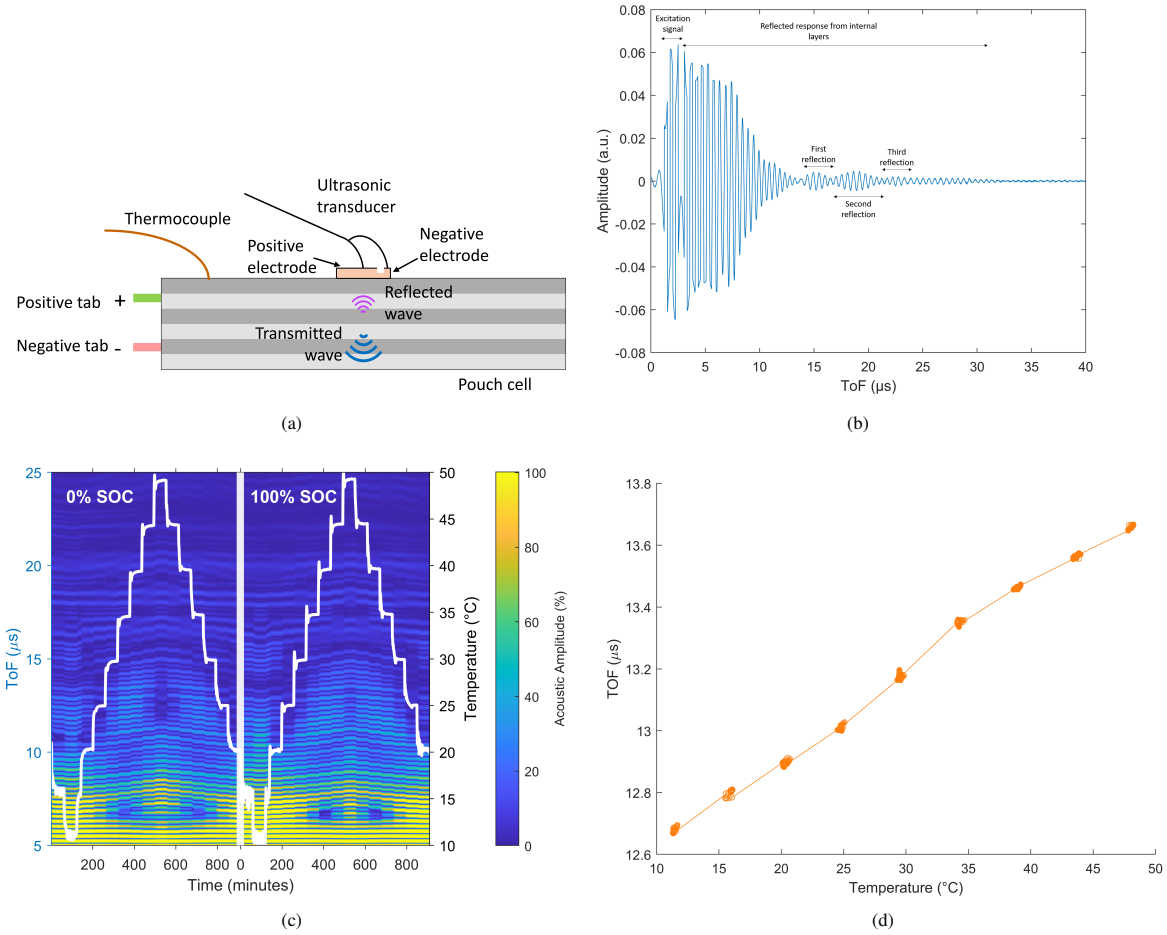

Figure 2: a) Schematic of ultrasonic monitoring setup for a LIB. b) The first three identifiable groups of acoustic reflections are highlighted. c) 3D plot comparison of a thermally cycled cell when fully discharged and fully charged, with temperature overlaid in black. d) a plot of the change in TOF of a single peak compared to the change in temperature.

one hour to ensure signal stability. With respect to temperature, the change in the TOF can be attributed to thermal expansion, which influences the TOF through two primary mechanisms: altering both the layer thickness (affecting acoustic travel path) and density.

The thickness of a material is inversely proportional to the density; as the thickness increases, the density decreases. The change in density affects the speed of sound through a material as defined in Equation 1, though our analysis suggests that the effect of the increased travel path outweighs the impact of the increased speed of sound when comparing the two SOCs presented in Figure 2c.

Figure 2c shows a comparison between the signals of a cell when fully discharged (left) and fully charged (right) during a thermal cycle. The comparison shows there are some notable changes, mainly in the amplitude of the peaks. Observing the TOF of the two signals, the peaks from the transducer runoff line up as expected, as they are mostly

unaffected by changes to the cell. From ca. 12 µs, slight offsets can be seen, which increase as the initial TOF increases. The changes observed are limited when compared to the influence of temperature.

In pursuit of a deeper understanding of the relationship between temperature and charge, we isolated selected peaks to plot the change in TOF through the cycles. First, the effect of temperature on a single acoustic peak at a constant SOC was plotted (Figure 2d). To ensure that temperature data from at least half of the cell was represented, under the assumption that the cell is mirrored across the acoustic barrier, the selected peak was taken from the first echo. A key observation is the linearity and reversibility of the plot; a positive correlation is seen between TOF and temperature. This is to be expected, given the volumetric thermal expansion α_v of a material is defined as

$$\alpha_v = \frac{1}{V}\frac{dV}{dT} \tag{6}$$

where V = volume (m^{-3}) - T = temperature (°C) and $\frac{dV}{dT}$ = rate at which the volume changes with respect to changes in temperature. The changes in volume, be it expansion when heating or contraction when cooled, changes the path length the ultrasonic signal must travel. If the cell heats up, the travel path increases, so the signal has to travel further to pass through the cell. The speed of sound through the material would also change, as the internal layers decrease in density. If during operation, the Young's modulus would also change with the movement of the ions between the electrodes. All these have an effect on the TOF.

Similar findings have been observed in other works [45, 46]. Following from this, the same peak was tracked across all tested SOC (Figure 3a). The results suggest the SOC has a negative correlation with the TOF, reducing the initial time as the cell is charged. This confirms the transducers were working as intended, as the negative correlation has been recorded multiple times within literature and has become the basis of this estimation technique [21, 47, 48].

We observe distinct patterns in the TOF measurements across the different SOC and temperatures states, with the most significant TOF change occurs between 0% and 20% SOC, with characteristic overlapping near 50% SOC that persists across all examined temperatures. These observations largely align with the known behaviour of thermal expansion in LIBs, which varies as a function of both temperature and SOC [49]. Although electrodes undergo phase changes during charge-discharge cycles that affect thermal expansion [50], these effects are minimal compared to ionic movement during operation [49].

Our observations indicate that thermal expansion exhibits quadratic behaviour at lower temperatures, transitioning to a more linear pattern at higher temperatures. Above 25 °C, the TOF shift with temperature displays more linear characteristics across most SOCs. This agrees with results found by [49], where cells with a similar jelly roll design saw non-linear thermal expansion below 25 °C, and linear expansion above 25 °C. The reasoning provided was that thermal expansion was linear, but at lower temperatures there is 'empty space' that the internal layers expand into,

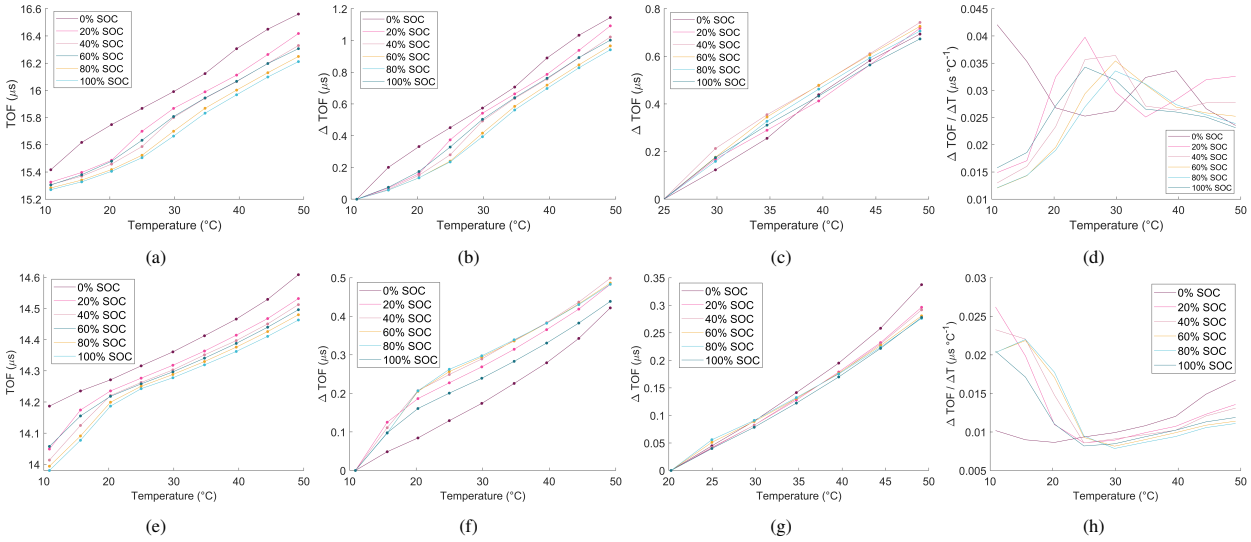

Figure 3: a) and b) TOF profile and subsequent change in TOF of selected peak the from the first reflection of Cell 1. c) presents the change in TOF of the peak from 25 °C as this is the temperature all SOC follow a similar trend. d) shows the gradient of the TOF changes across the SOC. e) - h) show the same for a random peak in Cell 2. g) shows from 20 °C for the same reasons as given for c).

providing the difference in observed expansion behaviours. As the relationship between the TOF and temperature appear to be proportional, an increase in thermal expansion would result in a proportional increase in TOF. The increase in the TOF is a direct result of the thermal expansion, as the travel path of the acoustic signal has increased with the increase in temperature.

Although Cell 1 exhibits an increasing slope as the temperature increases to 25 °C, Cell 2 demonstrates a flattening trend under similar conditions. Both cells show behaviour at 0% SOC in lower temperatures that deviate from the other SOC, with these patterns persisting until specific temperature thresholds - 20 °C for Cell 1 and 25 °C for Cell 2. Beyond these thresholds (Figures 3g and 3c), the SOCs show stronger alignment, with a greater response at the lower SOC attributed to increased thermal expansion [49]. Looking at the first-order differential of the TOF (Figures 3d and 3h) reveals that between 20% and 100% SOC, the gradients follow similar trends without discernible correlation with magnitude. The gradient patterns between cells mirror each other, though Cell 1's gradient (3d) is approximately double in magnitude compared to Cell 2's. These characteristic patterns, including the distinctive behaviour at 0% SOC and the temperature threshold transitions, are consistently observed in the gradient analysis.

The characteristics of thermal sensitivity differ significantly between cells, with Cell 2 (Figure 3e) showing a sharper increase in TOF between lower temperatures, except for 0% SOC as discussed earlier, before transitioning to a shallower increase at higher temperatures, contrasting with the behaviour of Cell 1. Despite these differences, both cells exhibit monotonic non-decreasing behaviour in temperature-TOF relationships. Examining the differential responses of the TOF (Figures 3b and 3f) highlights a distinct difference in behaviour between 0% SOC and all other

charge states, especially at lower temperatures. While the 20% to 100% SOCs exhibit consistent patterns across both cells (especially for Cell 2), the 0% SOC responses deviate significantly - displaying either contrary behaviour in Cell 1 or a greatly diminished response (Cell 2) from below 30 °C and 25 °C, respectively. This behaviour is clearly reflected in the absolute TOF measurements shown in Figures 3a and 3e.

3.2. Relationship between time-of-flight and temperature

As a linear relationship between temperature and the TOF has been shown for a peak (Figure 2d), this was confirmed using an AScan by comparing the ratio of the TOF of a peak at a given temperature to a reference temperature TOF_{ref}:

$$\frac{TOF}{TOF_{ref}} \tag{7}$$

In this case room temperature, 20 °C, was used as the reference temperature. The ratio for all cells, for all SOC are shown in Figure 4, where the solid lines represent the mean ratio, whilst the shaded areas represent the spread of the ratios across all peaks. The dotted lines mark the boundaries of the two standard deviation range.

The mean ratios represent the average values for all peaks identified in the AScan of each respective cell; for instance, the mean ratio at 50 °C and 0% SOC in Figure 4a represents the average of all peaks detected in that specific cell condition. The shaded area is defined by the largest and smallest ratio observed across all SOCs, showcasing the spread.

The figures demonstrate a linear relationship between TOF and temperature across all peaks in the tested cells, with each cell showing the same linear trend and slope as temperature increases, regardless of SOC. The mean square error (MSE) for all SOCs across all cells is presented in Figure S1, with the largest MSE (1.28×10^{-5}) occurring between 0% and 100% SOC for Cell 3. However, the slope is not consistent across cells, as seen in Figure 4d, where Cell 2 has a shallower slope compared to the other cells. Cells 1 and 3 show remarkable agreement in their gradients.

Despite the good agreement in the mean trends, the spread suggests a wide variation in measurements across the acoustic response.The ranges exhibit decreasing values as temperature approaches 20 °C (with the inverse occurring at other temperatures), although fluctuation amplitude varies between cells and temperature conditions; to evaluate the significance of this spread and validate the ratio's utility, we calculated two standard deviations for all trends (shown as dotted-dashed lines in Figures 4a, 4b and 4c). The shaded areas, which represent the maximum spread across all SOCs, are largely confined within two standard deviations, indicating a tight distribution of the ratios relative to a reference temperature near the mean values. For Cells 1 and 2, the standard deviations followed a similar trend to the data spread, albeit with a generally sharper slope. The viability of this ratio appears to improve as the temperature

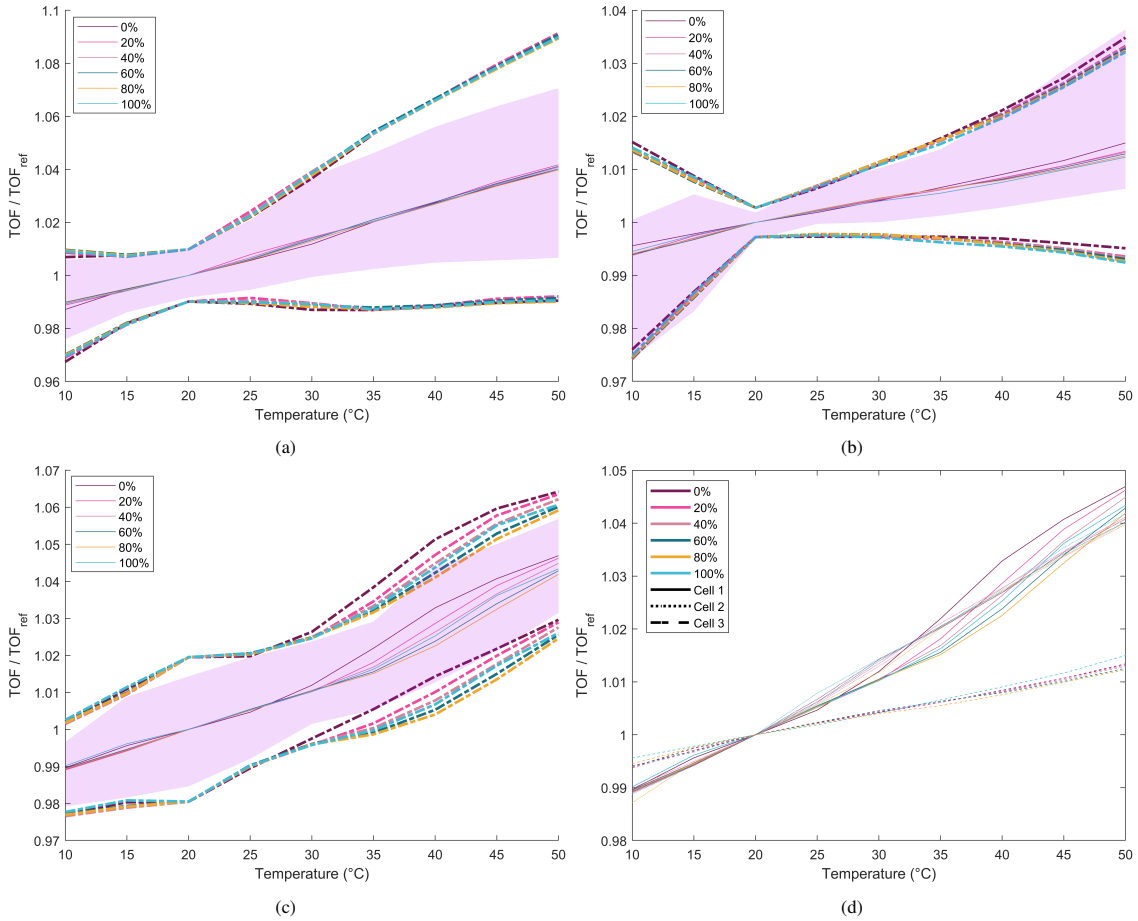

Figure 4: The ratio of TOFs (solid lines) for different SOC for a) Cell 1, b) Cell 2, and c) Cell 3, d) a comparison of the three cells. The pink shaded regions represent the spread of the ratios. The dotted lines enclose the regions within two standard deviations.

deviates from 20 °C. Meanwhile, Cell 3 saw a more linear pattern for the standard deviation, also similar to associated data spread. This was still constrained to within the two standard deviation however, showing the data spread is still tight around the mean values.

LIBs naturally undergo capacity fade through normal operation [51], which is accelerated through abusive operation or conditions such as high temperature. As the cell ages, the TOF is observed to undergo a shift that is independent of the change in SOC and temperature. This shift was found to increase or decrease, depending on the cell chemistry [30, 52]. The difference in TOF between fully charged and fully discharged as the cell degraded was negligible over 100 cycles of 300-cycle lifespan cells [28]. It could be hypothesised from this that this work that the ratio of TOF/TOF_{ref} could be consistent as the cell ages, though further experiments are needed to test this.

The physical, and therefore electrical, properties of a cell within a manufacturing batch are dependent on the production process, resulting in variations in the electrical properties of cells of the same manufacturing batch [51].

When comparing the ratios between cells in Figure 4d, this variation is observed as Cells 1 and 3 have comparable slopes, while Cell 2 has a shallower slope, but there is little variation between the SOCs within a cell. This variation in performance should be accounted for not only for acoustic monitoring, but as a general consideration when purchasing cells.

3.3. Sensitivity analysis

To delve deeper into the interaction and influence of the charge and temperature, we conducted a Global Sensitivity Analysis (GSA) using a variance-based decomposition to calculate the Sobol' indices [53]. This approach quantifies how input variables (in this case temperature and SOC) contribute to the output's variance both independently and through interaction. It decomposes the total variance into first-order effects (individual contributions of each input) and higher-order effects (interaction between inputs), calculating indices that represent the fraction of variance explained by each effect. Whilst we can see that both influence the acoustic signal, the individual effects of each are not clear; the acoustic signal is a superposition of the two variables. The co-dependent effect, or interaction between the two variables, is also unknown. Each output is a peak from the acoustic response, and the inputs are temperature and SOC. Each output had 54 data-points, as it was the combination of the nine temperature and six charge states. In order to present the data, each output in Figure 5 is an average across these 54 data-points

Although it is clear both temperature and state-of-charge (SOC) influence the acoustic signal, their individual and coupled effects are challenging to distinguish because of the superposition of their influences. Because the acoustic response changes result from both temperature and SOC variations, we treated each peak of the AScans as a separate output in our analysis. Given nine temperature and six charge states were measured, each output was an average of the combined 54 data points. When performing the analysis, the data is randomly divided into k subsets to apply k-fold cross-validation [54]. To balance between the number of data points per output and computational costs, the number of k-folds used was 27. Using a large number reduces the bias of a specific data subset. The sensitivity indices presented in Figure 5 represent the averages between these measurement points.

The results from the GSA are summarised in Figure 5, where the first order Sobol' indices for the charge and temperature influences on the TOF are presented. Across all three cells, temperature dominates the TOF changes compared to the SOC, which agrees with the results shown in Figure 3. The substantial difference in magnitude between input variables is noteworthy, with SOC accounting for merely 10% of ultrasonic variation, attributable to the narrow spacing observed between 20% and 100% SOC across the cells. There was an expected shift to a quicker TOF as the cells were charged, but this was overshadowed by the temperature, more noticeably in the higher temperature range (3c and 3g). A change of 10 °C would have the same effect on the TOF as full (dis)charging of the cell. This temperature difference could be achieved during normal operation [28], or exceeded if the C-rate is large

enough. The number of peaks vary between the cells due to the cells. Limited coordination between manufacturers results in variation in cell-to-cell manufacturing, such as the amount of active material and discontinuities within the active materials [28].

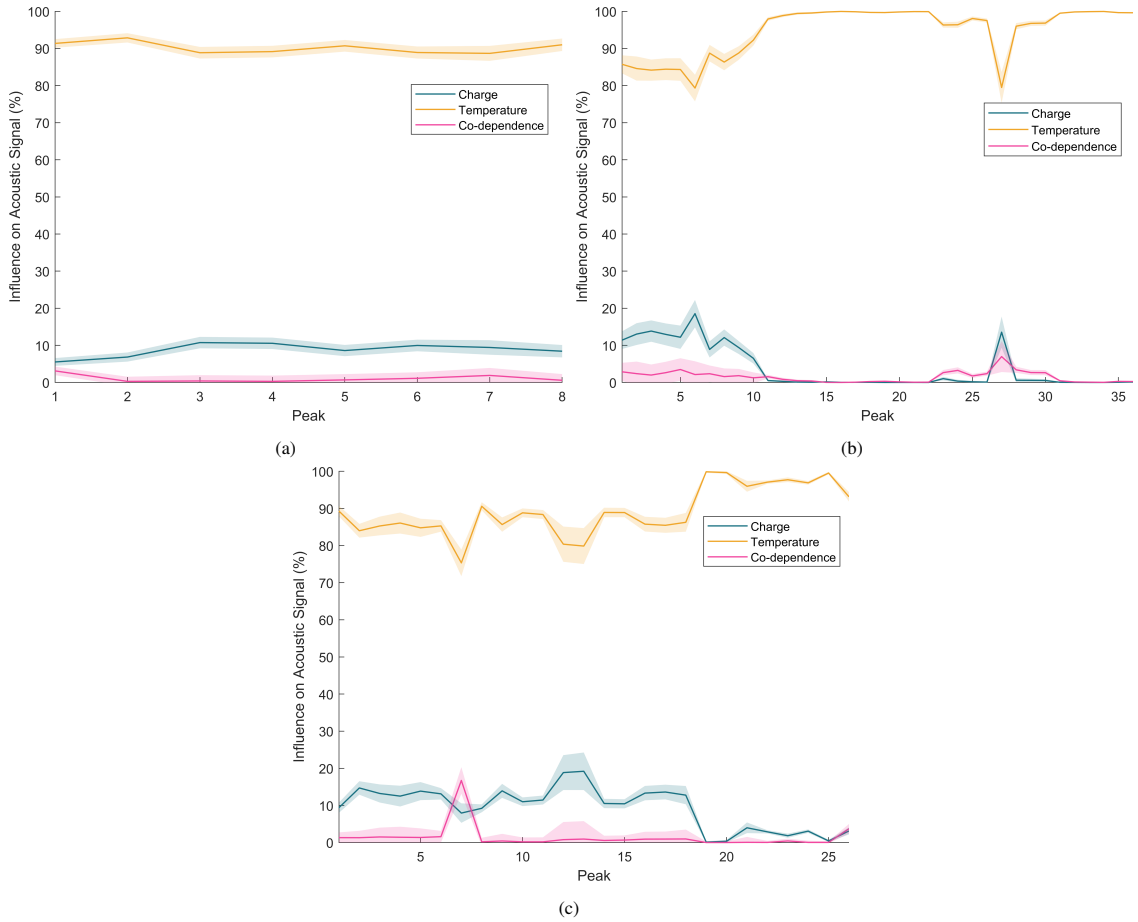

Figure 5: First-order Sobol' indices for charge (blue) and temperature (orange) for a) Cell 1, b) Cell 2, and c) Cell 3. The co-dependence (second-order) on the two inputs across the three cells are in pink.

Recall that the data shown in Figure 4 suggested insignificant influence from a combination of the charge and temperature. We used the GSA to confirm this co-dependent interactions by calculating the second-order Sobol' indices, looking at the second-order indices shows a similar result to the ratio of TOF to TOF_{ref}. The interaction between the two inputs has statistically zero effect on the TOF, evidencing that although temperature and charge individually influence the TOF, their interaction does not have a detectable impact. It should be stated that the internal heat generation from the resistance to ionic movement was not explored in this work, as the C-rate was kept low.

The shaded areas surrounding the first-order and second-order indices represent the uncertainty in our sensitivity measures, quantified as one standard deviation calculated through k-fold cross-validation analysis. These uncertainty

bounds remained consistently narrow across all three cells for both first-order and second-order indices, with each peak's standard deviation averaged across the individual outputs. The tight spread indicates statistical stability in our partitioning of the variance between temperature and SOC effects. This statistical robustness, demonstrated through repeated cross-validation sampling, validates both the performance of the model and the reliability of our sensitivity measurements, lending additional support to our findings of the dominating effect of temperature on the acoustic signal compared to the SOC.

4. Conclusion

Ultrasound has emerged as a valuable tool for monitoring battery performance, yielding information through transmission and reflection measurements of internal active materials. Although these investigations have resulted in significant developments, a deeper understanding of the discrete and coupled influences of thermal and SOC effects on the acoustic signal is required. In this work, a study was conducted on NMC lithium-ion cells to determine the influence of temperature and charge on the TOF of an ultrasonic acoustic signal. The results were collected through a thermal and charge cycle, allowing for a matrix of ultrasonic responses to different states of temperature and charge. We report significant effects of both temperature and charge, presenting evidence that temperature has a greater influence on the acoustic signal changes than charge. The question of co-dependency was also addressed. It was found that the interaction between temperature and charge is negligible and was significantly less than the individual influence of the two. We believe that our findings will bring attention to the mostly disregarded effects of temperature when using acoustics monitoring. Addressing this would accelerate the development of accurate acoustic LIB SOC estimations in tandem with current BMSs.

Work should be conducted to isolate the dominance of the influence of temperature to make this technology viable for industrial application. The temperature and SOC of a cell have statistically independent effects on the acoustic TOF, implying the isolation and decoupling of the two inputs should be possible, deconvoluting one from the other using a ratio similar to the method performed by Owen et al. [33]. However, this method requires a thermocouple throughout the use of the cell or a method for statistical inference.

In order to progress this work, further testing should be performed at higher C-rates, and with continuous cell charging/discharging, to investigate the co-dependency of internal heat generation as a result of the resistance to ionic movement during operation.

CRediT author statement

Daniel Williams: Conceptualisation, Data Curation, Formal Analysis, Investigation, Methodology, Visualisation, Writing - Original Draft, Writing - Review & Editing. **Robert Milton**: Formal Analysis, Visualisation. **Joshua**

Taylor: Formal Analysis, Visualisation. **Rob Dwyer-Joyce**: Supervision, Writing - Review & Editing. **Solomon Brown**: Supervision, Writing - Review & Editing.

Acknowledgements

The authors would like to thank the Faraday Institution (grant number FIRG028) and the Centre for Doctoral Training in Integrated Tribology (EP/L01629X/1) for their funding support of this work.

Data availability

The data is available from the corresponding author on reasonable request.

Declaration of of competing interest

The authors declare that they have no known competing financial interests or personal relationships that could have appeared to influence the work reported in this paper.

References

[1] X. Lai, M. Yuan, X. Tang, Y. Zheng, J. Zhu, Y. Sun, Y. Zhou, F. Gao, State-of-power estimation for lithium-ion batteries based on a frequency-dependent integer-order model, Journal of Power Sources 594 (2024). doi:10.1016/j.jpowsour.2023.234000.

[2] J. Yang, H. Zhang, Y. Xu, P. Li, Analysis of heat generation in lithium-ion battery components and voltage rebound based on electrochemical and thermal coupled model, Journal of Energy Storage 72 (2023). doi:10.1016/j.est.2023.108554.

[3] Y. Zheng, H. Wu, W. Yi, X. Lai, H. Dai, X. Han, M. Ouyang, A novel classification method of commercial lithium-ion battery cells based on fast and economic detection of self-discharge rate, Journal of Power Sources 478 (2020) 229039. doi:10.1016/j.jpowsour.2020.229039.

[4] B. Nykvist, M. Nilsson, Rapidly falling costs of battery packs for electric vehicles, Nature Climate Change 5 (2015). doi:10.1038/nclimate2564.

[5] Y. Ding, Z. P. Cano, A. Yu, J. Lu, Z. Chen, Automotive li-ion batteries: Current status and future perspectives, Nature Climate Electrochemical Energy Reviews 2 (2019). doi:10.1007/s41918-018-0022-z.

[6] W. R. Institute, World greenhouse gas emissions: 2020, [Accessed: 2024-06-18] (2023).
URL https://www.wri.org/data/world-greenhouse-gas-emissions-2020

[7] D. Doughty, E. Roth, A general discussion of li ion battery safety, Applied Energy (2012). doi:10.1149/2.F03122if.

[8] T. Reddy, Linden's Handbook of Batteries, McGraw-Hill Education, 2011.

[9] J. Xu, C. C. Mi, B. Cao, J. Deng, Z. Chen, S. Li, The state of charge estimation of lithium-ion batteries based on a proportional-integral observer, IEEE Transactions on Vehicular Technology 63 (2014). doi:10.1109/TVT.2013.2287375.

[10] Y. He, F. Ning, Q. Yang, Q. Song, B. Li, F. Su, H. Du, Z. Tang, F. Kang, Structural and thermal stabilities of layered $Li(Ni_{1/3}Co_{1/3}Mn_{1/3})O_2$ materials in 18650 high power batteries, Journal of Power Sources 196 (2011). doi:10.1016/j.jpowsour.2012.01.122.

[11] C. Truchot, M. Dubarry, B. Y. Liaw, State-of-charge estimation and uncertainty for lithium-ion battery strings, Applied Energy 119 (2014). doi:10.1016/j.apenergy.2013.12.046.

[12] K. W. E. Cheng, B. P. Divakar, H. Wu, K. Ding, H. F. Ho, Battery-management system (bms) and soc development for electrical vehicles, IEEE Transactions on Vehicular Technology 60 (2015). doi:10.1109/TVT.2010.2089647.

[13] W. Waag, C. Fleischer, D. U. Sauer, Critical review of the methods for monitoring of lithium-ion batteries in electric and hybrid vehicles, Journal of Power Sources 258 (2014). doi:10.1016/j.jpowsour.2014.02.064.

[14] A. Fotouhi, D. J. Auger, K. Propp, S. Longo, M. Wild, A review on electric vehicle battery modelling: From lithium-ion toward lithium–sulphur, Renewable and Sustainable Energy Reviews 56 (2016) 1008–1021.

[15] W. Li, D. Cao, D. Jöst, F. Ringbeck, M. Kuipers, F. Frie, D. U. Sauer, Parameter sensitivity analysis of electrochemical model-based battery management systems for lithium-ion batteries, Applied Energy 269 (2020) 115104.

[16] A. P. Schmidt, M. Bitzer, Á. W. Imre, L. Guzzella, Experiment-driven electrochemical modeling and systematic parameterization for a lithium-ion battery cell, Journal of Power Sources 195 (15) (2010) 5071–5080.

[17] M. A. Rahman, S. Anwar, A. Izadian, Electrochemical model parameter identification of a lithium-ion battery using particle swarm optimization method, Journal of Power Sources 307 (2016).

[18] J. Keil, A. Jossen, Electrochemical modeling of linear and nonlinear aging of lithium-ion cells, Journal of The Electrochemical Society 167 (11) (2020) 110535.

[19] B. Sood, C. Hendricks, M. Osterman, M. Pecht, Health monitoring of lithium-ion batteries, EDFA Technical Articles 16 (2014). doi:10.1109/ispce.2013.6664165.

[20] K. Ono, A comprehensive report on ultrasonic attenuation of engineering materials, including metals, ceramics, polymers, fiber-reinforced composites, wood, and rocks, Applied Sciences 10 (2020). doi:10.3390/app10072230.

[21] J. Chang, X. Zeng, T. Wan, Real-time measurements of lithium-ion batteries state-of-charge based on air-coupled ultrasound, AIP Advnaces 9 (2019). doi:10.1063/1.5108873.

[22] S. Sampath, X. Yin, Z. W. Tham, Y. F. Chen, L. Zhang, Real-time and non-contact estimation of state of charge for lithium-ion battery using laser ultrasonics, Journal of Power Sources 605 (2024) 234544. doi:10.1016/j.jpowsour.2024.234544.

[23] V. B. Shenoy, P. Johari, Y. Qi, Elastic softening of amorphous and crystalline li–si phases with increasing li concentration: a first-principles study, Journal of Power Sources 195 (19) (2010) 6825–6830. doi:10.1016/j.jpowsour.2010.04.044.

[24] Y. Qi, H. Guo, L. Hector, A. Timmons, Threefold increase in the young's modulus of graphite negative electrode during lithium intercalation, Journal of The Electrochemical Society 157 (2010). doi:10.1149/1.3327913.

[25] S. J. Harris, P. Lu, Effects of inhomogeneities – nanoscale to mesoscale – on the durability of li-ion batteries, The Journal of Physical Chemistry C 117 (13) (2013) 6481–6492. doi:10.1021/jp311431z.

[26] M. T. McDowell, S. W. Lee, W. D. Nix, Y. Cui, 25th anniversary article: understanding the lithiation of silicon and other alloying anodes for lithium-ion batteries, Advanced materials 25 (36) (2013) 4966–4985. doi:10.1002/adma.201301795.

[27] Y. Koyama, T. E. Chin, U. Rhyner, R. K. Holman, S. R. Hall, Y.-M. Chiang, Harnessing the actuation potential of solid-state intercalation compounds, Advanced Functional Materials 16 (4) (2006) 492–498. doi:10.1002/adfm.200500633.

[28] D. Williams, J. Green, P. Bugryniec, S. Brown, R. Dwyer-Joyce, Battery age monitoring: Ultrasonic monitoring of ageing and degradation in lithium-ion batteries, Journal of Power Sources 631 (2024). doi:https://doi.org/10.1016/j.jpowsour.2025.236174.

[29] P. Ladpli, R. Nardari, F. Kopsaftopoulus, Y. Wang, F. Chang, Design of multifunctional structural batteries with health monitoring capabilities, European Workshop on Structural Health Monitoring (2016).

[30] Y. Wu, Y. Wang, W. Yung, M. Pecht, Ultrasonic health monitoring of lithium-ion batteries, Electronics 8 (7) (2019). doi:10.3390/electronics8070751.

[31] J. Robinson, R. Owen, M. Kok, M. Maier, J. Majasan, M. Braglia, R. Stocker, T. Amietszajew, A. Roberts, R. Bhagat, D. Billsson, J. Olson, J. Park, G. Hinds, A. Tidblad, D. Brett, P. Shearing, Identifying defects in li-ion cells using ultrasound acoustic measurements, Journal of The Electrochemical Society 167 (12) (2020). doi:10.1149/1945-7111/abb174.

[32] M. Huang, N. Kirkaldy, Y. Zhao, Y. Patel, F. Cegla, B. Lan, Quantitative characterisation of the layered structure within lithium-ion batteries using ultrasonic resonance, Journal of Energy Storage 50 (2022) 104585. doi:10.1016/j.est.2022.104585.

[33] R. Owen, J. Robinson, J. Weaving, M. Pham, T. Tranter, T. Neville, D. Billson, M. Braglia, R. Stocker, A. Tidblad, P. Shearing, D. Brett, Operando ultrasonic monitoring of lithium-ion battery temperature and behaviour at different cycling rates and under drive cycle conditions, Journal of The Electrochemical Society (2022). doi:10.1149/1945-7111/ac6833.

[34] R. Owen, W. Wiśniewska, M. Braglia, R. Stocker, P. Shearing, D. Brett, J. Robinson, Operando ultrasonic monitoring of the internal temperature of lithium-ion batteries for the detection and prevention of thermal runaway, Journal of The Electrochemical Society 171 (2024). doi:10.1149/1945-7111/ad3beb.

[35] M. Appleberry, J. Kowalski, S. Africk, J. Mitchell, T. Ferree, V. Chang, V. Parekh, Z. Xu, Z. Ye, J. Whitacre, S. Murphy, Avoiding thermal runaway in lithium-ion batteries using ultrasound detection of early failure mechanisms, Journal of Power Sources (2022). doi:10.1016/j.jpowsour.2022.231423.

[36] R. Kazys, V. Vaskeliene, High temperature ultrasonic transducers: A review, Sensors 21 (2021). doi:10.3390/s21093200.

[37] V. Baran, O. Dolotko, M. Mühlbauer, A. Senyshyn, H. Ehrenberg, Thermal structural behavior of electrodes in li-ion battery studied in operando, Journal of The Electrochemical Society 165 (9) (2018) A1975. doi:10.1149/2.1441809jes.

[38] E. Lee, S. Muhammad, T. Kim, H. Kim, W. Lee, W.-S. Yoon, Tracking the influence of thermal expansion and oxygen vacancies on the thermal stability of ni-rich layered cathode materials, Advanced Science 7 (12) (2020) 1902413. doi:10.1002/advs.201902413.

[39] J. B. Robinson, M. Pham, M. D. R. Kok, T. M. M. Heenan, D. J. L. Brett, P. R. Shearing, Examining the cycling behaviour of li-ion batteries using ultrasonic time-of-flight measurements, Journal of Power Sources 444 (2019). doi:10.1016/j.jpowsour.2019.227318.

[40] H. Sun, N. Muralidharan, R. Amin, V. Rathod, P. Ramuhalli, I. Belharouak, Ultrasonic nondestructive diagnosis of lithium-ion batteries with multiple frequencies, Journal of Power Sources 549 (2022). doi:https://doi.org/10.1016/j.jpowsour.2022.232091.

[41] Q. Ke, S. Jiang, W. Li, W. Lin, X. Li, H. Huang, Potential of ultrasonic time-of-flight and amplitude as the measurement for state of charge and physical changings of lithium-ion batteries, Journal of Power Sources 549 (2022) 232031. doi:10.1016/j.jpowsour.2022.232031.

[42] D. Williams, R. Copley, P. Bugryniec, R. Dwyer-Joyce, S. Brown, A review of ultrasonic monitoring: Assessing current approaches to li-ion battery monitoring and their relevance to thermal runaway, Journal of Power Sources 590 (2024). doi:10.1016/j.jpowsour.2023.233777.

[43] R. Copley, D. Cumming, Y. Wu, R. Dwyer-Joyce, Measurements and modelling of the response of an ultrasonic pulse to a lithium-ion battery as a precursor for state of charge estimation, Journal of Energy Storage 36 (2021). doi:10.1016/j.est.2021.102406.

[44] R. A. Milton, Reduced Order Modelling using Global Sensitivity Analysis and Gaussian Process Regression (11 2017). doi:10.5281/zenodo.1234.
URL https://github.com/miltonra/RomCom

[45] H. N. G. Wadley, S. J. Norton, F. Mauer, B. Droney, E. A. Ash, C. M. Sayers, E. A. Ash, C. B. Scruby, Ultrasonic measurement of internal temperature distribution, Philosophical Transactions of the Royal Society of London. Series A, Mathematical and Physical Sciences 320 (1986). doi:10.1098/rsta.1986.0123.

[46] J. S. Slongo, J. Gund, T. A. R. Passarin, D. R. Pipa, J. E. Ramos, L. V. Arruda, F. N. Junior, Effects of thermal gradients in high-temperature ultrasonic non-destructive tests, Sensors 22 (2022). doi:10.3390/s22072799.

[47] A. G. Hsieh, S. Bhadra, B. J. Hertzberg, P. J. Gjeltema, A. Goy, J. W. Fleischer, D. A. Steingart, Electrochemical-acoustic time of flight: in operando correlation of physical dynamics with battery charge and health, Energy & Environmental Science 8 (5) (2015). doi:10.1039/c5ee00111k.

[48] L. Gold, T. Bach, W. Virsik, A. Schmitt, J. Müller, T. Staab, G. Sextl, Probing lithium-ion batteries' state-of-charge using ultrasonic transmission – concept and laboratory testing, Journal of Power Sources 343 (2017). doi:10.1016/j.jpowsour.2017.01.090.

[49] K. Oh, B. Epureanu, A novel thermal swelling model for a rechargeable lithium-ion battery cell, Journal of Power Sources 303 (2016). doi:10.1016/j.jpowsour.2015.10.085.

[50] V. Sethuraman, M. Chon, M. Shimshak, N. Van Winkle, P. Guduru, In situ measurement of biaxial modulus of si anode for li-ion batteries, Electrochemistry Communications 12 (2010). doi:10.1016/j.elecom.2010.09.008.

[51] D. Evans, D. M. Brieske, C. Tebruegge, J. Kowal, Analysis of the impact of manufacturing-induced cell-to-cell variation for high-power applications, Journal of Power Sources 614 (2024). doi:10.1016/j.jpowsour.2024.235001.

[52] P. Ladpli, F. Kopsaftopoulus, F. Chang, Estimating state of charge and health of lithium-ion batteries with guided waves using built-in piezoelectric sensors/actuators, Journal of Power Sources (2018). doi:10.1016/j.jpowsour.2018.02.056.

[53] S. R. Arwade, M. Moradi, A. Louhghalam, Variance decomposition and global sensitivity for structural systems, Engineering Structures 32 (1) (2010) 1–10. doi:10.1016/j.engstruct.2009.08.011.

[54] K. Konakli, B. Sudret, Global sensitivity analysis using low-rank tensor approximations, Reliability Engineering & System Safety 156 (2016). doi:10.48550/arXiv.1605.09009.